C-Terminal Truncated α-Synuclein Fibrils Contain Strongly Twisted β-Sheets

Iyer, A.; Roeters, S.J.; Kogan, V.; Woutersen, S.; Claessens, M.M.A.E.; Subramaniam, V.

DOI
10.1021/jacs.7b07403

Publication date
2017

Document Version
Final published version

Published in
Journal of the American Chemical Society

JACS JOURNAL OF THE AMERICAN CHEMICAL SOCIETY

Article

Cite This: J. Am. Chem. Soc. 2017, 139, 15392-15400

pubs.acs.org/JACS

C-Terminal Truncated α-Synuclein Fibrils Contain Strongly Twisted β-Sheets

Aditya Iyer,[†,§,#,∥] Steven J. Roeters,[‡,∥] Vladimir Kogan,[⊥] Sander Woutersen,[*,‡] Mireille M. A. E Claessens,[*,§] and Vinod Subramaniam[*,†,§,¶]

[†]Nanoscale Biophysics Group, AMOLF, Science Park 104, Amsterdam 1098 XG, The Netherlands

[‡]Van 't Hoff Institute for Molecular Sciences, University of Amsterdam, Science Park 904, Amsterdam 1098 XH, The Netherlands

[§]Nanobiophysics Group, MESA+ Institute for Nanotechnology, University of Twente, Drienerlolaan 5, Enschede 7522 NB, The Netherlands

[⊥]Dannalab BV, Wethouder Beversstraat 185, Enschede 7543 BK, The Netherlands

[¶]Vrije Universiteit Amsterdam, De Boelelaan 1105, Amsterdam 1081 HV, The Netherlands

Supporting Information

ABSTRACT: C-terminal truncations of monomeric wild-type alpha-synuclein (henceforth WT-αS) have been shown to enhance the formation of amyloid aggregates both *in vivo* and *in vitro* and have been associated with accelerated progression of Parkinson's disease (PD). The correlation with PD may not solely be a result of faster aggregation, but also of which fibril polymorphs are preferentially formed when the C-terminal residues are deleted. Considering that different polymorphs are known to result in distinct pathologies, it is important to understand how these truncations affect the organization of αS into fibrils. Here we present high-resolution microscopy and advanced vibrational spectroscopy studies that indicate that the C-terminal truncation variant of αS, lacking residues 109−140 (henceforth referred to as 1−108-αS), forms amyloid fibrils with a distinct structure and morphology. The 1−108-αS fibrils have a unique negative circular dichroism band at ∼230 nm, a feature that differs from the canonical ∼218 nm band usually observed for amyloid fibrils. We show evidence that 1−108-αS fibrils consist of strongly twisted β-sheets with an increased inter-β-sheet distance and a higher solvent exposure than WT-αS fibrils, which is also indicated by the pronounced differences in the 1D-IR (FTIR), 2D-IR, and vibrational circular dichroism spectra. As a result of their distinct β-sheet structure, 1−108-αS fibrils resist incorporation of WT-αS monomers.

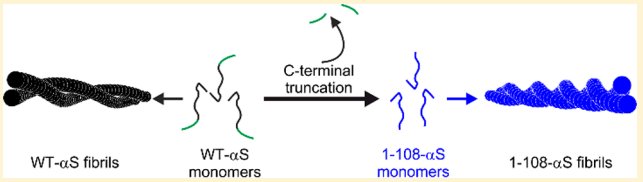

INTRODUCTION

Parkinson's disease (PD) is characterized by the presence of intracellular aggregates of fibrils of the intrinsically disordered protein alpha-synuclein (αS).[1−3] It is now well established that fibrillization of αS is involved in neuronal cell death in PD.[4,5] Wild-type αS (WT-αS) comprises three domains: the N-terminal region (residues 1−60), which is mainly involved in membrane binding,[6] the amyloidogenic NAC domain (residues 61−95), which is crucial for amyloid formation,[7] and the highly charged C-terminal region (residues 96−140), which is known to interact with polyamines, metal ions, and cellular proteins.[8] Although the cellular triggers for the self-assembly of monomeric αS into putatively toxic fibrillar aggregates are still unclear, it is evident that WT-αS can form different amyloid polymorphs: fibrils that differ in molecular structure and morphology.[9−13] These fibril polymorphs have been shown to induce distinct pathologies in cells and mice.[10,14]

Lewy bodies, a pathological hallmark of PD, not only contain fibrils consisting of WT-αS but also contain up to 15% truncated WT-αS variants.[15−17] Interestingly, the C-terminal αS truncation that is commonly found in Lewy bodies is also present in healthy brains and cultured cells.[16,21] Thus, αS truncation does not directly result in disease *per se*. However, experiments on transgenic mouse models, animal cell lines, and neuronal cells overexpressing C-terminally truncated αS show that there is strong correlation between C-terminal truncation variants and PD pathology.[18−23] Further, the *in vitro* produced aggregates of C-terminally truncated αS have also been shown to be more cytotoxic than WT-αS aggregates.[19,24,25]

Given the physiological relevance of this C-terminal truncation[19,24] and the role of αS-fibril polymorphism in disease,[9,11,12,26] we investigated the structure of fibrils of a C-terminal truncated variant of αS lacking residues 109−140[27] (1−108-αS). αS monomers are closely packed in the amyloid fibrils. The removal of amino acid residues from the highly charged solvent-exposed C-terminal region may have structural consequences arising from altered electrostatic and steric constraints. In amyloid fibrils, differences in the fold of monomers affect the fibril morphology and their physicochemical properties, which may translate to differences in cytotoxicity.[9,10,28] In spite of its importance and abundance,

Received: July 16, 2017
Published: October 2, 2017

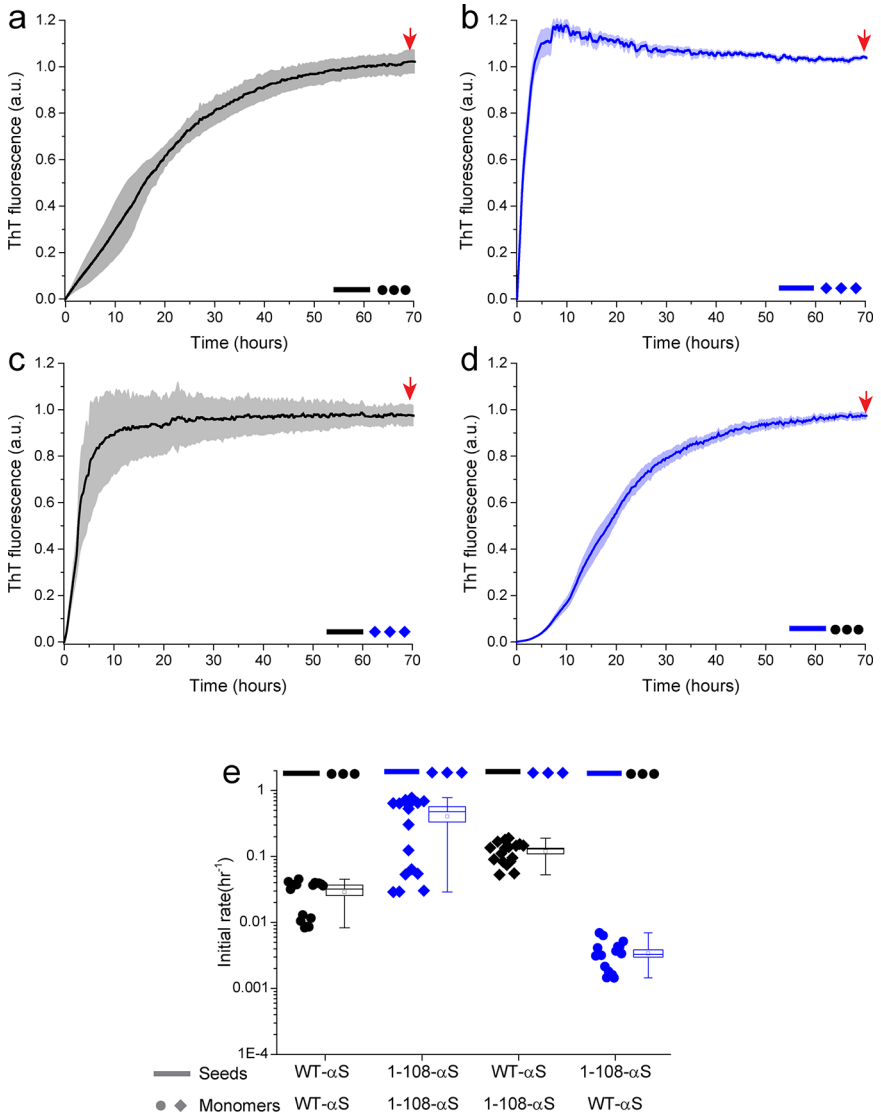

Figure 1. Seeding/cross-seeding profiles/rates of WT-αS (black circles) and 1−108-αS (blue diamonds). Representative aggregation profiles of monomeric WT-αS with WT-αS seeds (a), monomeric 1−108-αS with 1−108-αS seeds (b), monomeric 1−108-αS with WT-αS seeds (c), and monomeric WT-αS with 1−108-αS seeds (d), respectively. The monomer (circles for WT-αS and diamonds for 1−108-αS) concentration was 35 μM, and the seed (shown as bars) concentration was 1% (v/v) in PBS buffer at 37 °C. Shaded regions in panels a−d indicate SD from an aggregation experiment with at least 6 replicates. (e) Aggregation seeding rates obtained from a linear fit of the first 3000 s of the normalized seeded aggregation curves (Experimental Section) from three independent aggregation experiments. Red arrows in panels a−d refer to time-points at which samples were obtained for STEM images shown in Supporting Figure S2.

the influence of the C-terminal truncations on the resulting αS fibril structure is not well understood. Here we show how deletion of C-terminal residues of monomeric αS affects the structure, morphology, and surface properties of the resulting fibrils. Our experiments suggest that 1−108-αS fibrils are composed of strongly twisted β-sheets, resulting in fibrils wherein the intermolecular β-sheets are more solvent exposed compared to WT-αS fibrils. The formation of higher-ordered aggregates of fibrillar 1−108-αS follows from the increased hydrophobic exposure and the decreased charge repulsion between individual fibrils. The difference in fibril structure is confirmed in cross-seeding aggregation experiments, where we show that 1−108-αS fibrils cannot efficiently seed the aggregation of WT-αS monomers.

RESULTS AND DISCUSSION

The 1−108-αS Fibril Core Is Incompatible with the Addition of WT-αS Monomers. To investigate if the structure of 1−108-αS fibrils is distinctly different from WT-αS fibrils, the cross-seeding capabilities of WT-αS and 1−108-αS were tested. For this purpose, we performed aggregation experiments with thioflavin T (ThT). The addition of preformed αS fibrils, i.e., seeds, to αS monomers accelerates aggregation by bypassing primary nucleation processes.[29,30] Thus, by seeding a solution of monomers with preformed fibrils, information on the fibril growth is obtained and differences in fibril growth rate indicate structural differences in the fibril core.[9,31,32] A delay in (or absence of) seeding is indicative of an incompatible fibril core conformation. Homologous seeding (where seeds/monomers belong to the same αS variant) aggregation experiments using preformed

DOI: 10.1021/jacs.7b07403
J. Am. Chem. Soc. 2017, 139, 15392−15400

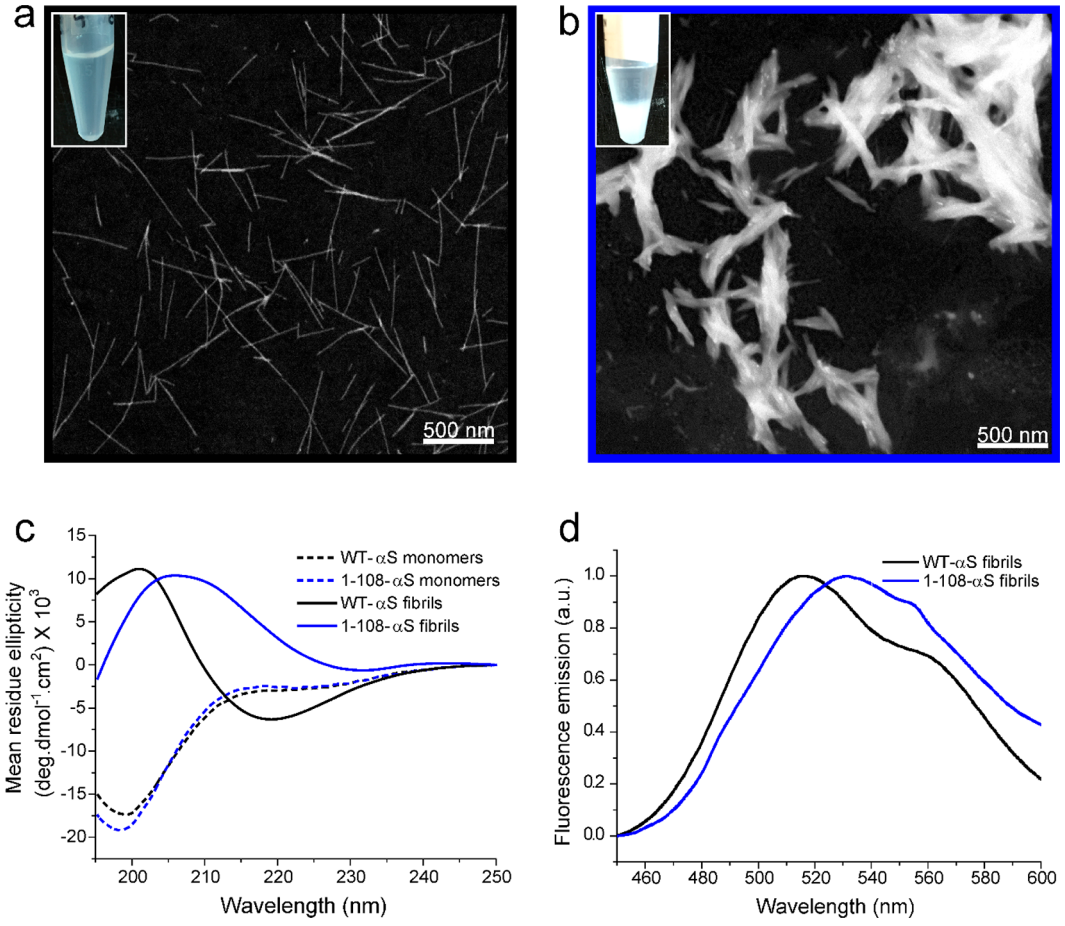

Figure 2. STEM micrographs (a, b), CD spectra (c), and FE fluorescence spectra (d) of WT-αS and 1−108-αS fibrils. Inset in panels a and b show suspensions of αS fibrils after 2 h. Settled aggregates of fibrils (densely white) are seen in the case of 1−108-αS fibrils only (b). Plotted data in c and d from WT-αS are depicted in black and that of 1−108-αS in blue. (c) CD spectra of WT-αS and 1−108-αS before (dotted lines) and after (solid lines) aggregation. Suspensions of fibrils were filtered to get rid of monomeric αS prior to measurement (Experimental Section). (d) Fluorescence emission spectra (λ_{exc} = 420 nm) of FE-dye interacting with αS fibrils showing that the short-emission N* band (~510 nm) is red-shifted for 1−108-αS fibrils with a higher band ratio of fluorescence emission peaks compared to the WT-αS fibrils.

seeds under identical buffer conditions show a faster incorporation of 1−108-αS monomers compared to WT-αS monomers (Figure 1a,b). WT-αS seeds are relatively more efficient in incorporating 1−108-αS monomers compared to WT-αS monomers (Figure 1a,c and black symbols in Figure 1e). The obtained rates for WT-αS monomers with 1−108-αS seeds were ~100-fold slower (Figure 1d and blue circles in Figure 1e) with a lag-time of ~3 h compared to those obtained from homologous seeding of 1−108-αS monomers (Figure 1b,d). Comparison of Figure 1d with unseeded aggregation data from WT-αS and 1−108-αS is shown in Supporting Figure S1.

1−108-αS Fibrils Are Composed of Strongly Twisted β-Sheets. The 100-fold slower incorporation of WT-αS monomers in 1−108-αS seeds is intriguing and probably results from a large difference in fibril structure. Unlike WT-αS fibrils that are visible as individual fibrils with twisted rod-like morphologies, 1−108-αS self-assembles into a mixed population of rod-like morphologies and aggregates of fibrils (Figure 2a,b), corroborating previous reports.[33] To understand these differences, we first investigated if the secondary structure of WT-αS and 1−108-αS in these aggregates differs. WT-αS and 1−108-αS monomers have similar UV-CD spectra that are characteristic of a disordered conformation, while the UV-CD spectra of their respective fibrillar aggregates differ significantly (Figure 2c). The UV-CD spectrum of the WT-αS fibrils contains a broad minimum at ~219 nm (arising from the n → π^* transition) typical for β-sheets, while the minimum of the 1−108-αS fibrils is red-shifted by ~11 nm, centering at ~230 nm. Compared to WT-αS fibrils, the positive maximum at ~200 nm (arising from the $\pi \rightarrow \pi^*$ transition) is also red-shifted by ~7 nm for the 1−108-αS fibrils. Both these shifts indicate possible differences in the protein secondary structure. When the aggregated 1−108-αS suspensions were left undisturbed in tubes for 2 h, a pellet of aggregates of fibrils settled, a process that was not observed for WT-αS suspensions (Figure 2a,b inset). The observed changes in intensity and center wavelength of UV-CD peaks for 1−108-αS fibrils could result from differential scattering or differential absorption flattening (DAF).[34,35] We excluded DAF effects by obtaining UV-CD spectra of both settled and suspended 1−108-αS fibrils and by comparing with another truncation variant of αS lacking residues 125−140 (1−124-αS)[33] (see Figures S3 and S4 and additional discussion in the Supporting Information).

A negative maximum in the UV-CD spectra at ~230 nm is typically assigned to high β-turn content in other proteins.[36,37] However, it is improbable that 1−108-αS fibrils are enriched in β-turns, as this would probably not result in a stable fibril

DOI: 10.1021/jacs.7b07403
J. Am. Chem. Soc. 2017, 139, 15392−15400

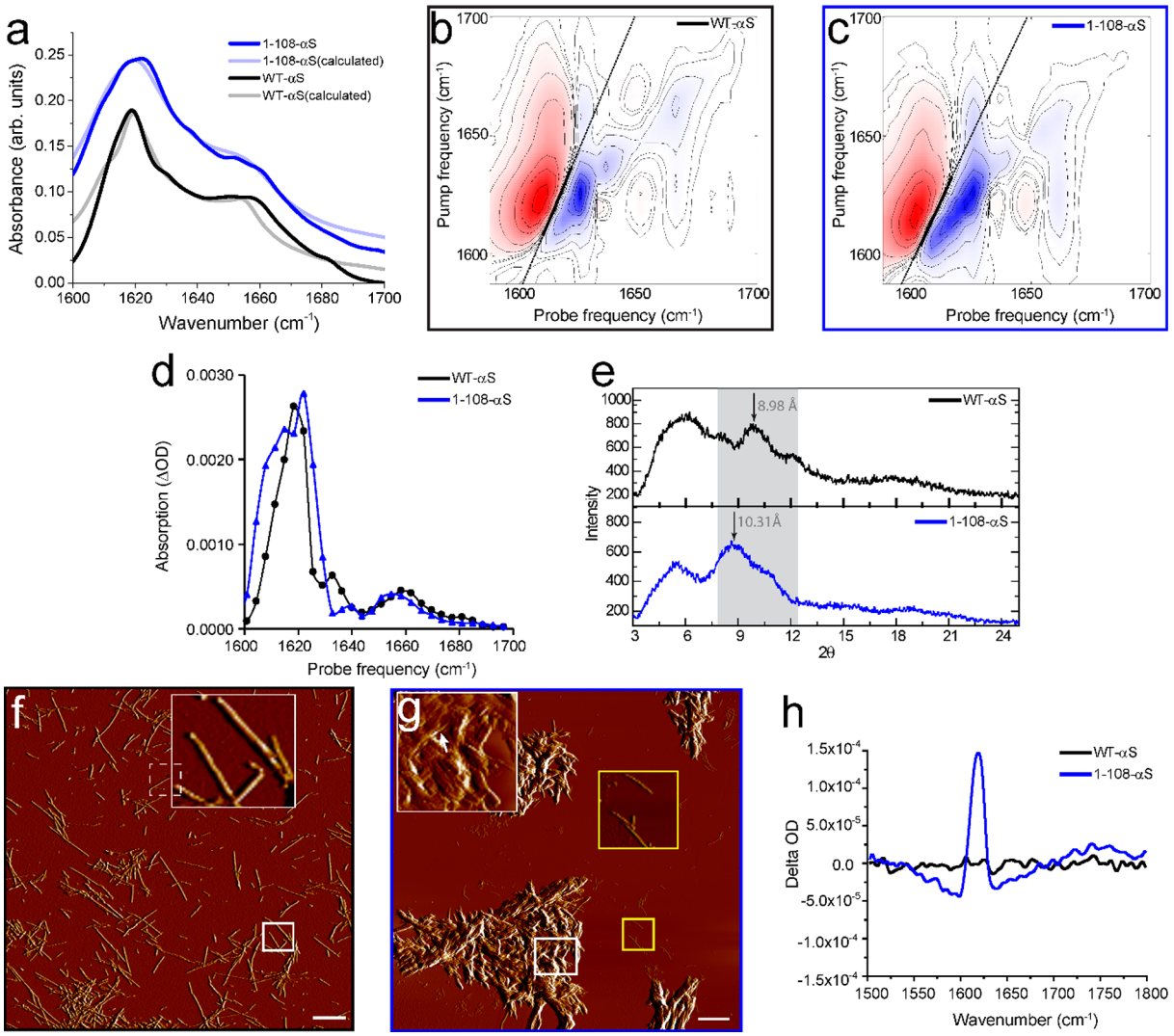

Figure 3. Structural characterization of WT-αS and 1−108-αS fibrils. All data from experiments with WT-αS are depicted in black and that of 1−108-αS in blue. (a) FTIR spectra of αS fibrils of the amide-I region. In gray and light blue are the calculated spectra as described in the text for an intersheet distance of 8.98 and 10.3 Å, respectively. (b, c) Perpendicular 2D-IR spectra of WT-αS (b), 1−108-αS fibrils (c), and their corresponding diagonal slices (d). (e) X-ray diffraction patterns of partially aligned αS fibrils depicting differences in the short-range reflections (arrows in gray background indicate peaks corresponding to intersheet distances) of WT-αS and 1−108-αS fibrils. (f, g) AFM amplitude images of αS fibrils on mica. Purified fibrils of WT-αS (f) show typical rod-like fibrillar morphology, while the 1−108-αS fibrils (g) show both higher-ordered fibrillar structures and sparse rod-like fibrils (insets). The scale bar is 1 μm. (h) VCD spectra of WT-αS and 1−108-αS fibrils.

structure. We speculate that a red-shift of the n → π* (215−219 nm) and π → π* transition region (195−200 nm) in UV-CD spectra of 1−108-αS fibrils could be a consequence of strongly twisted β-sheets,[38−40] as was reported recently for the ILQINS hexapeptide.[41] The presence of water molecules near the amide groups in the β-sheet fibril core may also explain the observed red-shifts in the UV-CD spectrum of the 1−108-αS fibrils, as electronic transitions of the amide group in β-sheets are affected by the solvent environment. For example, the wavelength of the $\pi\pi$* transition (much stronger than the nπ* transition) red-shifts in water as a result of hydrogen bonding to the nitrogen atom in the excited state. These hydrogen bonds can form in the excited state due to an intramolecular charge transfer from the amide-nitrogen to the amide-oxygen atom.[42] The increased polarity of the fibril surface was additionally confirmed using a polarity-sensitive fluorescent dye (Figure 2d). We recorded the fluorescence emission spectra of αS fibrils in the presence of 4′-(diethylamino)-3-hydroxyflavone (FE). Spectroscopic studies show that the environment of FE bound to αS fibrils is not hydrated, and that its fluorescence changes as a function of the polarity of its environment.[43,44] Compared to the FE fluorescence emission spectra of WT-αS fibrils, a prominent red-shift of the N* band in the 1−108-αS fibrils suggests that FE experiences a relatively polar environment in the latter (Figure 2d).

Vibrational Spectroscopy and XRD Reveal Differences in Molecular Structure. To obtain more structural information, we measured the 1D-IR (FT-IR) and 2D-IR spectra of WT-αS and 1−108-αS fibrils. WT-αS fibrils have an amide-I absorption spectrum with a sharp peak at ∼1620 cm^{-1}, indicating the presence of amyloid β-sheets, corroborating existing reports.[45−47]

The 1−108-αS fibrils have an FTIR spectrum with a broader low-frequency amide-I peak (Figure 3a). This broadening is more visible in the 2D-IR spectrum: the four distinct modes present in the WT-αS spectrum are smeared out in the 1−108-

DOI: 10.1021/jacs.7b07403
J. Am. Chem. Soc. 2017, 139, 15392−15400

Table 1. Quantitative Comparison of WT-αS and Truncated Variant Fibril Morphologies

fibril type	mean fibril height (nm)	# of fibrils, N	mean fibril periodicity (nm)	calculated net charge of monomer	fibril interstrand spacing from XRD (Å)
WT-αS	6.9 ± 0.9	56	95 ± 39	−9	8.98
1−108-αS	4.7 ± 0.9	74	52 ± 9	+3	10.31

αS spectrum, quantitatively reflected by an increase in the inverse slope of the line through the zero crossings of the low-frequency peak (solid lines in Figure 3b,c), which is a measure of the spectral heterogeneity[48] (0.47 ± 0.02 for the 1−108-αS fibrils compared to 0.42 ± 0.02 for the WT-αS fibrils). This larger spectral inhomogeneity can be caused by structural differences and/or by an increased exposure of the intermolecular β-sheets to water molecules in the 1−108-αS fibrils that lead to spectral broadening due to the broad distribution of hydrogen-bond lengths to the amide groups of the protein.[48−51] X-ray diffraction (XRD) spectra show that there are structural differences between the two types of fibrils. The most clearly visible difference is that the intersheet spacing is ∼15% larger for 1−108-αS than for WT-αS fibrils (Table 1 and Figure 3e).

Spectral calculations indicate that the observed changes in IR spectra are a result of both the increased solvent exposure of the intermolecular β-sheets and the increased intersheet spacing. We calculate the spectra by employing a one-exciton model that incorporates different coupling models for nearest- and non-nearest neighbors, as well as hydrogen-bond-induced local-mode frequency shifts[52] on *in silico* constructed αS-like fibrils based on the crystal structure of the fibril formed by the 68−78 segment of αS (Experimental Section). The changed through-space coupling, resulting from the increased intersheet distance in 1−108-αS fibrils, leads to a more intense low-frequency mode at ∼1610 cm^{-1} (see Supporting Figure S5). A normal-mode analysis reveals that the smaller through-space coupling results in a typical $\nu_{\perp}$ mode of an isolated parallel β-sheet,[53,54] which is stronger than the normal mode that causes the shoulder in the more tightly packed fibril structure, as in the latter case the proximity of the neighboring sheets perturbs the relative phase of the local-mode oscillators. In the experimental spectra, this peak is most visible in the diagonal of the 2D-IR spectrum (Figure 3d) because highly delocalized normal modes (like amyloid modes) have a relatively higher intensity in 2D-IR spectra. The experimentally observed broadening of the 1−108-αS spectrum compared to the WT-αS spectrum is not reproduced fully by matching the intersheet distance of the *in silico* constructed 1−108-αS-like fibril to the value found in the XRD spectrum of 1−108-αS fibrils. Therefore, we think that the broadening is a result of the increased solvent exposure of the intermolecular β-sheets, which causes the aforementioned broader distribution of hydrogen bonds to water molecules, as has been observed before for amyloid fibrils that have water-exposed intermolecular β-sheets.[51] If we simulate this effect by doubling the line width for 1−108-αS as compared to WT-αS, add a disordered structure peak in the β-sheet/disordered structure ratio as determined by NMR,[55] and include a 3 cm^{-1} frequency shift between the two spectra (this shift may be due to small differences in the environment of the amide groups besides the hydrogen bonding with water), we obtain the gray and light-blue spectrum depicted in Figure 3a. The three main peaks (at ∼1620, 1657, and 1685 cm^{-1}) are reproduced by the model, allowing a structural assignment to be made. The 1620 and 1685 cm^{-1} peaks indeed result from the presence of β-sheets, and the 1657 cm^{-1} peak results from the presence of turns. Another aspect of 2D-IR that can be used to study the molecular structure are the off-diagonal cross-peaks that are sensitive to the orientation and distance between the different vibrational modes. The fact that the cross-peak pattern is not very different for WT-αS and 1−108-αS indicates a similarity in molecular structure and suggests that the relative orientation and distance between the β-sheet and turn peaks do not differ much. The largest differences are the $(\nu_{probe}, \nu_{pump})$ = (1657, 1620) cm^{-1} cross-peak that is extended to lower wavenumbers and the (1685, 1620) cm^{-1} cross-peak that is much weaker for 1−108-αS fibrils. The former is a direct result of the increased intensity of the low-frequency shoulder of the 1620 cm^{-1} peak, whereas the latter is probably a result of the broadening due to the increased water solvent exposure of the intermolecular β-sheets that results in a more smeared out and thus harder to observe cross-peak.

Additional Structural Differences Revealed by AFM and VCD. The difference in the β-sheet structure between WT-αS and 1−108-αS translates into morphological differences between the fibrils at larger length scales. These larger-scale differences were assessed by atomic force microscopy (AFM). WT-αS fibrillation results in sparse networks of individual fibrils that have an average height of ∼6.9 nm (Table 1) similar to previous reports,[56] while fibrils of 1−108-αS organize in fibrillar aggregates that were extremely heterogeneous in heights, ranging between ∼50 and 400 nm (Figure 3f,g).

The spatially separated individual 1−108-αS fibrils have an average height of ∼4.7 nm. Measurements of fibril periodicities, the helical pitch of twisted fibrils, show that 1−108-αS fibrils are nearly twice as twisted as WT-αS fibrils.

To further investigate the difference in supramolecular structure between WT-αS and 1−108-αS fibrils, we recorded vibrational circular dichroism (VCD) spectra (Figure 3h). There is a strong correlation between chiral (supra)molecular structure and the VCD signal.[57] Fibrils of 1−108-αS show a so-called "giant VCD" signal (in this case, a $\Delta\varepsilon/\varepsilon$ ratio of 3×10^{-3}) that is comparable to values observed for other mature amyloid fibrils,[57−67] while there is no detectable VCD signal for WT-αS fibrils. This might be either due to a difference in the (supra)molecular chirality or due to the size of the aggregates that, when of the same order as (or larger than) the vibrational wavelength (∼6 μm), can lead to a strong enhancement of the VCD signal, as has been observed before for liquid crystals.[68,69]

Concluding Remarks. Altogether, the biophysical and structural measurements show that αS molecules in 1−108-αS fibrils adopt a different conformation than in WT-αS fibrils. The inter-β-sheet distances are larger in the more-twisted 1−108-αS fibrils than in the less-twisted WT-αS fibrils, which probably results in an increased solvent exposure of the intermolecular β-sheets in 1−108-αS fibrils compared to WT-αS fibrils. Individual β-strands in canonical β-sheets are typically twisted right-handedly along the polypeptide chain axis due to chirality of the α-carbon atoms in proteins.[39,70,71] Besides the intrinsic chirality of the carbon atoms, also the relatively long and highly negatively charged C-terminal tails of αS affect the orientation of the residues in the fibril. The negatively charged, unstructured C-terminal region is respon-

DOI: 10.1021/jacs.7b07403
J. Am. Chem. Soc. 2017, 139, 15392−15400

sible for electrostatic interactions; the net interprotein repulsion is expected to be highest between WT-αS monomers and between WT-αS monomers and WT-αS fibrils and significantly less so for the truncated 1−108-αS species. This difference in interprotein repulsion is likely, at least in part, responsible for the ∼2-fold smaller nucleation time and the ∼10-fold higher homologous aggregation rate for 1−108-αS monomers compared to WT-αS monomers. The repulsion between the highly negatively charged C-terminal tails of αS monomers in the fibril affects the orientation of the residues in the fibril. In the WT-αS fibril, the twist of the fibril likely minimizes electrostatic repulsions between adjacent C-terminal regions of WT-αS with respect to other energetic constraints, thereby accommodating the charged C-terminal chains. Heterologous aggregation experiments indicate that the accommodation of WT-αS monomers in the 1−108-αS fibril structure is problematic. The elongation of 1−108-αS fibrils by WT-αS monomers is possibly inhibited by the placement of the unstructured, charged C-terminal residues of the WT-αS monomers in the 1−108-αS fibril structure. We speculate that the twisting of the β-sheets in 1−108-αS fibrils and/or the relative orientation of the monomers is incompatible with the presence of the C-terminal region and thus prevents fibril elongation. This problem does not exist for the addition of 1−108-αS monomers, lacking the C-terminal region, to WT-αS fibrils leading to much faster heterologous addition (black symbols of Figure 1e). The absence of the C-terminal tail in 1−108-αS reduces the energetic penalty associated with the close packing of the 32-amino acid long charged C-terminal region that is present in WT-αS fibrils, but increases the entropic penalty resulting from exposure of the hydrophobic NAC region. Together these constraints could be responsible for the change in the twist of the β-sheets in the 1−108-αS fibrils compared to WT-αS observed by AFM.

The extent of twisting in a β-sheet arises from the tendency of the system to minimize its free energy.[40] Nontwisted strands found in β-sheets lie on the diagonal ($\langle\phi + \psi\rangle = 0°$) ($\phi$ and ψ are the dihedral angles of rotation between the N−C_α and C_α−C bonds in a peptide bond) in a Ramachandran plot, while right-handed twisted strands in β-sheets ($\langle\phi + \psi\rangle > 10°$) lie right of the diagonal.[71,72] The increase in the twist of the β-sheets in the 1−108-αS fibrils (so that $\langle\phi + \psi\rangle > 10°$) can lead directly to increased intersheet distances observed in the XRD measurements, which is supported by increased solvent exposure indicated by the FE fluorescence emission spectra. The changes in the intersheet distance and chain twist result in direct contact of a larger surface of the β-sheet segments with the solvent. This increased contact can explain the observed changes in the 1D- and 2D-IR spectra.

The aggregation of αS with single-point mutations[73] and chemical modifications[50,74] can result in structurally and morphologically different fibrillar species. Existing evidence shows that differences in WT-αS fibril morphology can have varying cytotoxic effects.[9,10] Studies have shown that 1−108-αS fibrils are more cytotoxic[75] compared to WT-αS fibrils. Although C-terminally truncated forms of αS are common in PD[15−17] and other truncated proteins are also implicated in the pathogenesis of other neurodegenerative diseases such as Alzheimer's[76] and Huntington's[77] disease, it remains unclear whether protein truncations are directly responsible for cell death in these diseases. The presence of truncated proteins in pathological aggregates can be a result of either pre- or post-aggregation cleavage by proteases. Since cleavage drastically alters the surface properties of the fibrils, even post-aggregation cleavage may be harmful since the resulting exposure of the hydrophobic surface may result in nonspecific binding of other essential cellular proteins with hydrophobic domains.

EXPERIMENTAL SECTION

Expression Purification of αS Variants. All αS variants were expressed in *Escherichia coli* strain BL21(DE3) using the pT7-7 expression plasmid and purified in the presence of 1 mM DTT as previously reported.[78]

Preparation of αS Fibrils. For every protein variant, a final concentration of 35 μM of monomeric protein was allowed to aggregate in PBS (137 mM NaCl, 3 mM KCl, 10 mM phosphate) buffer at 37 °C under constant shaking at 300 rpm in LoBind polypropylene tubes from Eppendorf. Prior to aggregation assays, all prepared protein samples were filtered using a 100 kDa membrane to remove any pre-existing aggregates, and protein concentration was estimated using UV absorbance. Residual monomers after aggregation were separated using a 100 kDa filter and were always <10% of starting concentration for all variants used. The purified fibrils were thereafter used for measurements. For 2D-IR measurements, D_2O was used instead of H_2O and prior to measurements, and residual monomers were removed via ultracentrifugation at ∼10000*g*.

Thioflavin T Aggregation Assay. ThT-based αS aggregation assays were carried out on polystyrene microplates in a TECAN Infinite M200 microplate reader at a ThT concentration of 5 μM. Aggregation was carried out using 1% seeds at 37 °C using 35 μM αS monomers in PBS buffer. Seeds were prepared by sonicating freshly prepared and filtered (using a 100 kDa filter) αS fibrils in PBS buffer for 5 min. Two independent measurements were performed each with at least six replicates. The initial aggregation rate was determined by measuring the increase in ThT fluorescence within the first 3000 s of the measurement.[79]

Scanning Transmission Electron Microscopy (STEM). Freshly prepared fibrils were diluted with Milli-Q water and then prepared for STEM dark-field imaging. Typically, a 5 μL drop of 20 μM fibril samples was adsorbed on 300 mesh Formvar-coated copper grids for 5 min and then washed five times with water. The grid was air-dried at 37 °C and then transferred under vacuum into the STEM setup. Before recording the dark-field STEM micrographs, condenser stigmators were adjusted to give a circular beam profile, and the beam was carefully centered and spread to produce uniform illumination over the field of view. Dark-field digital micrographs of fibrils were acquired using a FEI Verios 460 microscope operating at 20 kV electron beam energy and 50 pA current.

Atomic Force Microscopy. For AFM measurements, 20 μL of the 10 μM fibril suspension was incubated on freshly cleaved mica (15 × 15 mm) for 5 min. Samples were thereafter washed with Milli-Q water and dried using N_2 gas. Thereafter, the samples were kept in 37 °C for 1 h to remove any residual water. AFM images were acquired in tapping mode on a Dimension 3100 scanning probe microscope (Bruker) using NSG01 gold probes (resonant frequency between 87 and 230 kHz and a tip radius <10 nm) in ambient air conditions. Fibril heights were measured using NanoScope Analysis v1.5 software and for the measurements of fibril periodicities, fibrils in AFM images were traced using a custom-written script in MATLAB using the DIPimage toolbox (version 2.3, TU Delft, Delft, The Netherlands).[80] Periodicity measurements were performed only on fibrils greater than 0.5 μm in length.

Circular Dichroism (CD) Spectroscopy. A Chirascan CD spectrometer was used to obtain UV-CD spectra of αS fibrils prepared in PBS buffer at an effective protein concentration of 10 μM. This was measured as follows: after measurement of fibril UV-CD spectra, 30% 1,1,1,3,3,3-Hexafluoro-2-propanol (HFIP) was added to the fibril suspension and shaken for 5 min. By measuring mean residue ellipticity (MRE) values for known concentrations of monomeric αS obtained after addition of 30% HFIP and shaking, a standard curve of UV-CD signals versus monomer concentration was generated. From this curve, unknown concentrations of 30% HFIP-solubilized fibrils

DOI: 10.1021/jacs.7b07403
J. Am. Chem. Soc. 2017, 139, 15392−15400

were estimated. Fibril samples were first purified using a 100 kDa cutoff filter to remove monomeric protein. Spectra were recorded between 195 and 260 nm with a step size of 1 nm and a scanning speed of 10 nm/min using a 1 mm path length cuvette at room temperature.

Sample Preparation for IR Spectroscopy. αS monomers were lyophilized overnight in a ScanVac Coolsafe (Labogene) to remove H_2O and resuspended in PBS buffer prepared in D_2O. Subsequently they were purified using a 100 kDa cutoff filter to remove any pre-existing aggregates and then kept under constant shaking at 300 rpm at 37 °C. Before measurements, αS fibril samples were again purified using a 100 kDa cutoff filter to remove monomeric protein. The final concentration for each IR sample was ∼150 μM. A 15 μL amount of fibril solution was placed between two 2 mm thick CaF_2 windows with a 50 μm spacer.

1D- and 2D-IR and VCD Spectroscopy. Each 1D-IR (FTIR) spectrum was an average of 32 scans, measured on a Bruker Vertex 70. The VCD spectra were also measured on this spectrometer, specifically by using the PMA 50 polarization modulation accessory, averaging for 210 min, while the IR cell was continuously rotated in order to remove any contribution from a nonrandom orientation of the fibrils in the sample cell. The 2D-IR spectra were measured on a setup described elsewhere.[81] In short, a commercially available mode-locked Ti:sapphire oscillator system whose output is amplified by a Ti:sapphire regenerative amplifier was used to create ∼50 fs, 800 nm pulses of ∼3.1 mJ at a repetition rate of 1 kHz. These were converted in an optical parametric amplifier into ∼100 fs, ∼6100 nm pulses of ∼20 μJ with an approximately Gaussian distribution with a full width at half-maximum (fwhm) of ∼150 cm^{-1}. The IR beam was then split into a pump, probe, and a reference beam. The pump beam is led through a Fabry-Pérot interferometer and thereby reduced in bandwidth to a fwhm of ∼12 cm^{-1}. The pump polarization was then rotated 90° with respect to the probe polarization by a $\lambda/2$ plate (in order to measure the perpendicular 2D-IR spectra) and subsequently overlapped with the probe pulse in the sample in a ∼200 μm focus. All spectra were obtained at a pump−probe delay of 1.5 ps, at room temperature. The heterogeneity of the low-frequency β-sheet mode was estimated by calculation of the inverse slope of the line through the zero crossings. In order to do this, we first determined the frequencies where the signal goes through zero, between the induced absorption (red peak at lower probe frequency) and the bleach (blue peak at higher probe frequency), for each pump pixel in the 1600−1625 cm^{-1} region by interpolation of the data point just before and just after the zero crossing, after which we fitted a straight line through the interpolated zero crossings.

Steady-State Fluorescence Spectroscopy. The emission spectra of FE dye was obtained with a Cary Eclipse spectrofluorimeter (Varian). Spectral slits were set at 5 nm, and samples were excited at 420 nm. Fluorescence emission spectra were recorded from 450 to 600 nm at room temperature using a 10 mm path cuvette after incubation of FE dye for 1 h with αS fibrils in PBS buffer. Experiments were performed in triplicates at final concentrations of 20 μM αS fibrils and 2 μM FE dye.

X-ray Fiber Diffraction. X-ray fiber diffraction (Philips X'Pert-MPD system with a Cu Kα wavelength of 1.5418 Å in reflection θ–θ mode) was used to analyze the structure of αS fibrils (∼4 mg/mL of purified fibrils) deposited on a monocrystal substrate with the surface nonparallel to crystalline planes, with a beam stop mounted on top of the sample. During the measurements, the sample was rotated at 4 s/revolution. The diffractometer was operated at 40 kV, 40 mA at a 2θ range of 2−40° employing a step size of 0.025°. The weak signal in the 4−7 Å region is possibly a result of the presence of 137 mM NaCl in our PBS buffers, which may affect the alignment of fibrils. A parallel alignment of most fibrils to the crystal surface may render the β-sheet distance largely invisible. Peaks in the 4−7 Å region are seen in the absence of NaCl.[13]

■ ASSOCIATED CONTENT

Supporting Information

The Supporting Information is available free of charge on the ACS Publications website at DOI: 10.1021/jacs.7b07403.

The five supporting images, supporting discussion, and supporting references (PDF)

■ AUTHOR INFORMATION

Corresponding Authors

*s.woutersen@uva.nl
*m.m.a.e.claessens@utwente.nl
*v.subramaniam@vu.nl

ORCID

Aditya Iyer: 0000-0002-3144-6385
Vinod Subramaniam: 0000-0001-6712-7266

Present Address

#Membrane Enzymology Group, Groningen Institute of Biomolecular Sciences & Biotechnology, University of Groningen, Groningen, The Netherlands.

Author Contributions

‖A. Iyer and S. J. Roeters contributed equally to the presented work.

Notes

The authors declare no competing financial interest.

■ ACKNOWLEDGMENTS

The authors thank Nathalie Schilderink and Kirsten van Leijenhorst-Groener for assistance in protein expression and purification and Prof. Roberta Croce from the VU University Amsterdam and Prof. J. Antoinette Killian from the Utrecht University for access to the CD spectrometer. The authors also thank Dr. Volodymyr Shvadchak for discussions and for providing the polarity-sensitive FE dye. The work presented here is part of a project titled "A Single Molecule View on Protein Aggregation" (No. 127) funded by the Foundation for Fundamental Research on Matter (FOM), now merged with The Netherlands Organisation for Scientific Research (NWO). We also acknowledge support from NanoNextNL, a micro- and nanotechnology consortium of the Government of The Netherlands and 130 partners. S.J.R. and S.W. acknowledge the European Research Council (ERC) for funding through grant 210999 and The Netherlands Organization for Scientific Research (NWO) for financially supporting this research.

■ REFERENCES

(1) Breydo, L.; Wu, J. W.; Uversky, V. N. *Biochim. Biophys. Acta, Mol. Basis Dis.* **2012**, *1822*, 261−285.
(2) Stefanis, L. *Cold Spring Harbor Perspect. Med.* **2012**, *2*, 1−23.
(3) Eisenberg, D.; Jucker, M. *Cell* **2012**, *148*, 1188−1203.
(4) Wong, Y. C.; Krainc, D. *Nat. Med.* **2017**, *23*, 1−13.
(5) Singh, S. K.; Dutta, A.; Modi, G. *Future Med. Chem.* **2017**, *9*, 1039−1053.
(6) Zarbiv, Y.; Simhi-Haham, D.; Israeli, E.; Elhadi, S. A.; Grigoletto, J.; Sharon, R. *Neurobiol. Dis.* **2014**, *70*, 90−98.
(7) Waxman, E. A.; Mazzulli, J. R.; Giasson, B. I. *Biochemistry* **2009**, *48*, 9427−9436.
(8) Eliezer, D. *J. Mol. Biol.* **2013**, *425*, 2393−2396.
(9) Bousset, L.; Pieri, L.; Ruiz-Arlandis, G.; Gath, J.; Jensen, P. H.; Habenstein, B.; Madiona, K.; Olieric, V.; Bockmann, A.; Meier, B. H.; Melki, R. *Nat. Commun.* **2013**, *4*, 2575.

DOI: 10.1021/jacs.7b07403
J. Am. Chem. Soc. 2017, 139, 15392−15400

(10) Peelaerts, W.; Bousset, L.; Van der Perren, A.; Moskalyuk, A.; Pulizzi, R.; Giugliano, M.; Van den Haute, C.; Melki, R.; Baekelandt, V. *Nature* **2015**, *522*, 340−344.
(11) Annamalai, K.; Guhrs, K. H.; Koehler, R.; Schmidt, M.; Michel, H.; Loos, C.; Gaffney, P. M.; Sigurdson, C. J.; Hegenbart, U.; Schonland, S.; Fandrich, M. *Angew. Chem., Int. Ed.* **2016**, *55*, 4822−4825.
(12) Tycko, R. *Neuron* **2015**, *86*, 632−645.
(13) Roeters, S. J.; Iyer, A.; Pletikapic, G.; Kogan, V.; Subramaniam, V.; Woutersen, S. *Sci. Rep.* **2017**, *7*, 41051.
(14) Woerman, A. L.; Stohr, J.; Aoyagi, A.; Rampersaud, R.; Krejciova, Z.; Watts, J. C.; Ohyama, T.; Patel, S.; Widjaja, K.; Oehler, A.; Sanders, D. W.; Diamond, M. I.; Seeley, W. W.; Middleton, L. T.; Gentleman, S. M.; Mordes, D. A.; Sudhof, T. C.; Giles, K.; Prusiner, S. B. *Proc. Natl. Acad. Sci. U. S. A.* **2015**, *112*, E4949−4958.
(15) Baba, M.; Nakajo, S.; Tu, P. H.; Tomita, T.; Nakaya, K.; Lee, V. M.; Trojanowski, J. Q.; Iwatsubo, T. *Am. J. Pathol.* **1998**, *152*, 879−884.
(16) Lucking, C. B.; Brice, A. *Cell. Mol. Life Sci.* **2000**, *57*, 1894−1908.
(17) Beyer, K.; Ariza, A. *Mol. Neurobiol.* **2013**, *47*, 509−524.
(18) Games, D.; Valera, E.; Spencer, B.; Rockenstein, E.; Mante, M.; Adame, A.; Patrick, C.; Ubhi, K.; Nuber, S.; Sacayon, P.; Zago, W.; Seubert, P.; Barbour, R.; Schenk, D.; Masliah, E. *J. Neurosci.* **2014**, *34*, 9441−9454.
(19) Li, W.; West, N.; Colla, E.; Pletnikova, O.; Troncoso, J. C.; Marsh, L.; Dawson, T. M.; Jakala, P.; Hartmann, T.; Price, D. L.; Lee, M. K. *Proc. Natl. Acad. Sci. U. S. A.* **2005**, *102*, 2162−2167.
(20) Ulusoy, A.; Febbraro, F.; Jensen, P. H.; Kirik, D.; Romero-Ramos, M. *Eur. J. Neurosci* **2010**, *32*, 409−422.
(21) Choi, D. H.; Kim, Y. J.; Kim, Y. G.; Joh, T. H.; Beal, M. F.; Kim, Y. S. *J. Biol. Chem.* **2011**, *286*, 14168−14177.
(22) Kanda, S.; Bishop, J. F.; Eglitis, M. A.; Yang, Y.; Mouradian, M. M. *Neuroscience* **2000**, *97*, 279−284.
(23) Ritchie, C. M.; Thomas, P. J. *Health* **2012**, *04*, 1167−1177.
(24) Muntane, G.; Ferrer, I.; Martinez-Vicente, M. *Neuroscience* **2012**, *200*, 106−119.
(25) Sung, J. Y.; Park, S. M.; Lee, C. H.; Um, J. W.; Lee, H. J.; Kim, J.; Oh, Y. J.; Lee, S. T.; Paik, S. R.; Chung, K. C. *J. Biol. Chem.* **2005**, *280*, 25216−25224.
(26) Covell, D. J.; Robinson, J. L.; Akhtar, R. S.; Grossman, M.; Weintraub, D.; Bucklin, H. M.; Pitkin, R. M.; Riddle, D.; Yousef, A.; Trojanowski, J. Q.; Lee, V. M. *Neuropathol. Appl. Neurobiol.* **2017**, DOI: 10.1111/nan.12402.
(27) Fernandez, C. O.; Hoyer, W.; Zweckstetter, M.; Jares-Erijman, E. A.; Subramaniam, V.; Griesinger, C.; Jovin, T. M. *EMBO J.* **2004**, *23*, 2039−2046.
(28) Mahul-Mellier, A. L.; Vercruysse, F.; Maco, B.; Ait-Bouziad, N.; De Roo, M.; Muller, D.; Lashuel, H. A. *Cell Death Differ.* **2015**, *22*, 2107−2122.
(29) Buell, A. K.; Galvagnion, C.; Gaspar, R.; Sparr, E.; Vendruscolo, M.; Knowles, T. P.; Linse, S.; Dobson, C. M. *Proc. Natl. Acad. Sci. U. S. A.* **2014**, *111*, 7671−7676.
(30) Yagi, H.; Kusaka, E.; Hongo, K.; Mizobata, T.; Kawata, Y. *J. Biol. Chem.* **2005**, *280*, 38609−38616.
(31) Sidhu, A.; Segers-Nolten, I.; Subramaniam, V. *ACS Chem. Neurosci.* **2016**, *7*, 719−727.
(32) Ono, K.; Takahashi, R.; Ikeda, T.; Yamada, M. *J. Neurochem.* **2012**, *122*, 883−890.
(33) Hoyer, W.; Cherny, D.; Subramaniam, V.; Jovin, T. M. *Biochemistry* **2004**, *43*, 16233−16242.
(34) Wallace, B. A.; Lees, J. G.; Orry, A. J.; Lobley, A.; Janes, R. W. *Protein Sci.* **2003**, *12*, 875−884.
(35) Castiglioni, E.; Abbate, S.; Longhi, G.; Gangemi, R.; Lauceri, R.; Purrello, R. *Chirality* **2007**, *19*, 642−646.
(36) Momotani, Y.; Arie, R.; Takagi, T. *Biochim. Biophys. Acta, Protein Struct.* **1981**, *668*, 193−196.
(37) Smith, J. A.; Pease, L. G. *Crit. Rev. Biochem.* **1980**, *8*, 315−399.
(38) Manning, M. C.; Illangasekare, M.; Woody, R. W. *Biophys. Chem.* **1988**, *31*, 77−86.
(39) Weatherford, D. W.; Salemme, F. R. *Proc. Natl. Acad. Sci. U. S. A.* **1979**, *76*, 19−23.
(40) Salemme, F. R. *Prog. Biophys. Mol. Biol.* **1983**, *42*, 95−133.
(41) Lara, C.; Reynolds, N. P.; Berryman, J. T.; Xu, A.; Zhang, A.; Mezzenga, R. *J. Am. Chem. Soc.* **2014**, *136*, 4732−4739.
(42) Nielsen, E. B.; Schellman, J. A. *J. Phys. Chem.* **1967**, *71*, 2297−2304.
(43) Celej, M. S.; Caarls, W.; Demchenko, A. P.; Jovin, T. M. *Biochemistry* **2009**, *48*, 7465−7472.
(44) Klymchenko, A. S.; Demchenko, A. P. *Phys. Chem. Chem. Phys.* **2003**, *5*, 461−468.
(45) Conway, K. A.; Harper, J. D.; Lansbury, P. T., Jr. *Biochemistry* **2000**, *39*, 2552−2563.
(46) Rochet, J. C.; Conway, K. A.; Lansbury, P. T., Jr. *Biochemistry* **2000**, *39*, 10619−10626.
(47) Ramakrishnan, M.; Jensen, P. H.; Marsh, D. *Biochemistry* **2006**, *45*, 3386−3395.
(48) Hamm, P.; Zanni, M. T. *Concepts and Methods of 2D Infrared Spectroscopy*; Cambridge University Press: New York, 2011.
(49) Manas, E. S.; Getahun, Z.; Wright, W. W.; DeGrado, W. F.; Vanderkooi, J. M. *J. Am. Chem. Soc.* **2000**, *122*, 9883−9890.
(50) Iyer, A.; Roeters, S. J.; Schilderink, N.; Hommersom, B.; Heeren, R. M.; Woutersen, S.; Claessens, M. M.; Subramaniam, V. *J. Biol. Chem.* **2016**, *291*, 21110−21122.
(51) Kim, Y. S.; Liu, L.; Axelsen, P. H.; Hochstrasser, R. M. *Proc. Natl. Acad. Sci. U. S. A.* **2009**, *106*, 17751−17756.
(52) Roeters, S. J.; van Dijk, C. N.; Torres-Knoop, A.; Backus, E. H.; Campen, R. K.; Bonn, M.; Woutersen, S. *J. Phys. Chem. A* **2013**, *117*, 6311−6322.
(53) Abramavicius, D.; Mukamel, S. *J. Chem. Phys.* **2004**, *120*, 8373−8378.
(54) Ganim, Z.; Chung, H. S.; Smith, A. W.; Deflores, L. P.; Jones, K. C.; Tokmakoff, A. *Acc. Chem. Res.* **2008**, *41*, 432−441.
(55) Gath, J.; Bousset, L.; Habenstein, B.; Melki, R.; Bockmann, A.; Meier, B. H. *PLoS One* **2014**, *9*, e90659.
(56) Sidhu, A.; Segers-Nolten, I.; Subramaniam, V. *Biochim. Biophys. Acta, Proteins Proteomics* **2014**, *1844*, 2127−2134.
(57) Kurouski, D.; Lu, X.; Popova, L.; Wan, W.; Shanmugasundaram, M.; Stubbs, G.; Dukor, R. K.; Lednev, I. K.; Nafie, L. A. *J. Am. Chem. Soc.* **2014**, *136*, 2302−2312.
(58) Ma, S.; Cao, X.; Mak, M.; Sadik, A.; Walkner, C.; Freedman, T. B.; Lednev, I. K.; Dukor, R. K.; Nafie, L. A. *J. Am. Chem. Soc.* **2007**, *129*, 12364−12365.
(59) Kurouski, D.; Dukor, R. K.; Lu, X.; Nafie, L. A.; Lednev, I. K. *Biophys. J.* **2012**, *103*, 522−531.
(60) Schwartz, E.; Liegeois, V.; Koepf, M.; Bodis, P.; Cornelissen, J. J.; Brocorens, P.; Beljonne, D.; Nolte, R. J.; Rowan, A. E.; Woutersen, S.; Champagne, B. *Chem. - Eur. J.* **2013**, *19*, 13168−13174.
(61) Aparicio, F.; Nieto-Ortega, B.; Najera, F.; Ramirez, F. J.; Lopez Navarrete, J. T.; Casado, J.; Sanchez, L. *Angew. Chem., Int. Ed.* **2014**, *53*, 1373−1377.
(62) Shanmugam, G.; Polavarapu, P. L. *Biochim. Biophys. Acta, Proteins Proteomics* **2013**, *1834*, 308−316.
(63) Dzwolak, W.; Kalinowski, J.; Johannessen, C.; Babenko, V.; Zhang, G.; Keiderling, T. A. *J. Phys. Chem. B* **2012**, *116*, 11863−11871.
(64) Measey, T. J.; Smith, K. B.; Decatur, S. M.; Zhao, L.; Yang, G.; Schweitzer-Stenner, R. *J. Am. Chem. Soc.* **2009**, *131*, 18218−18219.
(65) Shanmugam, G.; Polavarapu, P. L. *J. Struct. Biol.* **2011**, *176*, 212−219.
(66) Nieto-Ortega, B.; Nebot, V. J.; Miravet, J. F.; Escuder, B.; Navarrete, J. T.; Casado, J.; Ramirez, F. J. *J. Phys. Chem. Lett.* **2012**, *3*, 2120−2124.
(67) Schwartz, E.; Vdovin, A.; Koepf, M.; Buma, W. J.; Cornelissen, J. J. L. M.; Rowan, A. E.; Nolte, R. J. M.; Woutersen, S.; Domingos, S. R. *Macromolecules* **2010**, *43*, 7931−7935.
(68) Holzwarth, G.; Chabay, I.; Holzwarth, N. A. W. *J. Chem. Phys.* **1973**, *58*, 4816−4819.

DOI: 10.1021/jacs.7b07403
J. Am. Chem. Soc. 2017, 139, 15392−15400

(69) Holzwarth, G.; Holzwarth, N. A. W. *J. Opt. Soc. Am.* **1973**, *63*, 324−331.
(70) Chothia, C. *J. Mol. Biol.* **1973**, *75*, 295−302.
(71) Chothia, C. *J. Mol. Biol.* **1983**, *163*, 107−117.
(72) Chothia, C.; Janin, J. *Biochemistry* **1982**, *21*, 3955−3965.
(73) Nielsen, S. B.; Macchi, F.; Raccosta, S.; Langkilde, A. E.; Giehm, L.; Kyrsting, A.; Svane, A. S.; Manno, M.; Christiansen, G.; Nielsen, N. C.; Oddershede, L.; Vestergaard, B.; Otzen, D. E. *PLoS One* **2013**, *8*, e67713.
(74) Qin, Z.; Hu, D.; Han, S.; Reaney, S. H.; Di Monte, D. A.; Fink, A. L. *J. Biol. Chem.* **2007**, *282*, 5862−5870.
(75) Opazo, F.; Krenz, A.; Heermann, S.; Schulz, J. B.; Falkenburger, B. H. *J. Neurochem.* **2008**, *106*, 529−540.
(76) Sisodia, S. S.; St George-Hyslop, P. H. *Nat. Rev. Neurosci.* **2002**, *3*, 281−290.
(77) Ross, C. A. *Neuron* **2002**, *35*, 819−822.
(78) van Raaij, M. E.; Segers-Nolten, I. M.; Subramaniam, V. *Biophys. J.* **2006**, *91*, L96−98.
(79) Shvadchak, V. V.; Claessens, M. M.; Subramaniam, V. *J. Phys. Chem. B* **2015**, *119*, 1912−1918.
(80) Faas, F. G.; Rieger, B.; van Vliet, L. J.; Cherny, D. I. *Biophys. J.* **2009**, *97*, 1148−1157.
(81) Huerta-Viga, A.; Shaw, D. J.; Woutersen, S. *J. Phys. Chem. B* **2010**, *114*, 15212−15220.

DOI: 10.1021/jacs.7b07403
J. Am. Chem. Soc. 2017, 139, 15392−15400